Journal of Water Process Engineering 63 (2024) 105561

Contents lists available at ScienceDirect

Journal of Water Process Engineering

journal homepage: www.elsevier.com/locate/jwpe

Power feasibility of single-staged full-scale PRO systems with hypersaline draw solutions

A. Ruiz-García

Department of Electronic Engineering and Automation, University of Las Palmas de Gran Canaria, Campus Universitario de Tafira, E-35017 Las Palmas de Gran Canaria, Spain

ARTICLE INFO

Editor: Sadao Araki

Keywords:
Osmotic power
Pressure retarded osmosis
Blue energy
Renewable energy
Optimization

ABSTRACT

Pressure retarded osmosis (PRO) is a process that allow to generate energy from osmotic gradient. This process uses selective membranes in order to produce electrical energy through a hydraulic turbine. PRO can be used as a renewable energy technology where water resources are inexhaustible. PRO has the advantage of knowing when and how much energy will be produced. Unfortunately at the moment there are certain limiting factors concerning membrane and module characteristics that have prevented PRO to be fully exploited at full-scale. This study aims to assess the impact of hypersaline draw solutions (60–180 g L^{-1}), membrane characteristics such as structural parameter, module membrane surface and permeability coefficients on the net energy generated by single-staged full-scale PRO system with up to 8 spiral wound membrane modules (SWMMs) in series in a pressure vessel. To carry out this study, characteristics of existing PRO membranes at lab-scale were scaled up to 8 inches SWMM. The results showed the change in the optimal operating parameters with the change of membrane characteristics and draw solution concentration. This study concluded that single-staged full-scale PRO process would be viable from an energy point of view if membranes were manufactured on an industrial scale and with the characteristics of existing membranes on a laboratory scale.

1. Introduction

The electrical energy generation mainly depends on fossil fuels, which has a negative impact on the environment such as greenhouse gases emissions. To remedy this problem, power generation through the use of renewable energy sources (RES) such as wind, solar, wave, etc. is being promoted [1]. One of the main challenges that these RES have is its intermittent and unpredictable nature, which makes it difficult to integrate in large quantities [2,3]. Blue energy obtained from osmotic gradient has been proposed as alternative RES whose generatable energy is predictable. Several technologies that can enable the generation of electrical energy from the osmotic gradient are currently being investigated [4]. These technologies include pressure retarded osmosis (PRO), which is a process that uses semi-permeable membranes with high solute rejection to generate osmotic power [5–7]. Electric power generation would be produced by a hydraulic turbine at the outlet of the dilute stream [8]. Reversed electrodialysis (RED) is another membrane process that uses ion exchange membranes and can directly transform the energy produced by solutions of different concentration into electricity without any other auxiliary equipment [9,10]. Thermo-osmotic energy conversion (TOEC) is a technology based on the thermo-osmosis mechanism that involves the migration of a fluid through a semi-permeable membrane due to the thermal gradient. This process, like the PRO, requires a hydraulic turbine to generate electricity [11,12]. Of these technologies, PRO has proven to be the one with the highest power density (*PD*) [13–15]. Unfortunately, the vast majority of the studies carried out are on a laboratory scale, and the main challenge of the process is to prove its viability on full-scale [16,17]. To do so, it is necessary to estimate the performance of such systems taking into account the characteristics of the membrane elements [18] and the factors that attenuate their performance on full-scale [19–21].

There are two main membrane configurations, hollow fiber (HF) and SWMM (rolled flat sheet) [22]. The viability of PRO systems is strongly dependent on the characteristics of the membranes. These characteristics are mainly the water and solute permeability coefficients (*A* and *B*, respectively) [18] and the resistance to fouling. In addition to these intrinsic characteristics of the membrane material, there are others related to the module, such as the spacer geometry, which has impact on Δp and on the ECP, the structural parameter (*S*) which has impact on the ICP and the packing density of the membrane, i.e. S_m. Much effort is being put into improving the efficiency of PRO membranes. For example, through the use of different nanomaterials such as zeolite, graphene oxide, carbon nanotubes, halloysite nanotubes, etc. [6,23,24].

E-mail address: alejandro.ruiz@ulpgc.es.

https://doi.org/10.1016/j.jwpe.2024.105561
Received 20 January 2024; Received in revised form 5 May 2024; Accepted 27 May 2024
Available online 3 June 2024

Nomenclature

Acronyms

DS	draw solution
ECP	external concentration polarization
ERD	energy recovery device
FS	feed solution
HF	hollow fiber
ICP	internal concentration polarization
PV	pressure vessel
RES	renewable energy sources
RO	reverse osmosis
SRES	steady renewable energy sources
SWMM	spiral wound membrane module
SWRO	seawater reverse osmosis
TFC	thin-film composite

Variables

$\dot{m}$	mass flow (kg s^{-1})
A	water permeability coefficient (m Pa^{-1} s^{-1})
A_0	initial water permeability coefficient (m Pa^{-1} s^{-1})
B	solute permeability coefficient (m s^{-1})
CF	concentration factor
C	concentration (g L^{-1} or kg (solute) kg^{-1} (water))
DF	dilution factor
D	solute diffusivity (m^2 s^{-1})
d_h	hydraulic diameter of feed channel (m)
FF	fouling factor
H	spacer height (m)
h	specific enthalpy (J kg^{-1})
J	flux per unit area (m^3 m^{-2} s^{-1})
K	solute resistivity (s m^{-1})
k	mass transfer coefficient
K_λ	parameter applied to friction factor
L	length of the SWMM (m)
n	number of SWMMs in PRO system
PD	power density (W m^{-2})
P	power (W)
p	pressure (Pa)
P_{ew}	wall Péclet number
Q	flow (m^3 h^{-1} or m^3 s^{-1})
R	flux recovery (%)
S	structural parameter (μm)
Sc	Schmidt number
Sh	Sherwood number
S_m	membrane surface area (m^2)
TCF	temperature correction factor
T	temperature (°C or K)

Greek letters

$\Delta\pi$	osmotic pressure difference (Pa)
Δp	pressure drop (Pa)
η	performance
γ	lumped parameter
μ	dynamic viscosity (Pa s)
ν	velocity (m s^{-1})
π	osmotic pressure (Pa)
ρ	density (kg m^{-3})
ε	porosity in feed channel
ϑ	specific volume m^3 kg^{-1}

Subscripts

av	average
boost	booster
D	draw
F	feed
id	ideal
in	input
m	membrane
out	output
p	permeate
TB	turbine
x	draw or feed

She et al. [25] assessed the impact of three different feed spacer geometries on a flat sheet membrane made of cellulose triacetate. The obtained an A coefficient of 4.17×10^{-12}, 4×10^{-12} and 2.78×10^{-12} m Pa^{-1} s^{-1}, and the corresponding values for B coefficients were 6.11×10^{-7}, 5.69×10^{-7} and 2.22×10^{-7} m s^{-1}. 716, 757 and 686 μm were the values obtained for S. An optimization of a thin-film nanofiber composite PRO flat sheet membrane with a specific support structure was done by Song et al. [26]. The optimum A and B values were 1.14×10^{-12} m Pa^{-1} s^{-1} and 4.83×10^{-7} m s^{-1}, respectively. A S value of 135 μm was obtained, it should be remarked that this is the lowest value of S for flat sheet membranes found in the literature. Two nanofiber composite PRO flat sheet membranes were made and tested by Bui and McCutcheon [27]. A S value of 273 μm was determined and RO tests to calculate A and B were carried out and obtained values of 1.47×10^{-11} and 7.86×10^{-12} m Pa^{-1} s^{-1} for A, 1.38×10^{-6} and 1.22×10^{-7} m s^{-1} for B. Cui et al. [28] made TFC flat sheet membranes with a polyamide thin film layer via interfacial polymerization and a macrovoid-free polyamide support. They obtained an A value 7.69×10^{-12} m Pa^{-1} s^{-1}, B value 3.31×10^{-7} m s^{-1} and S value 503 μm. Li et al. [29] manufactured and assess TFC polyetherimide flat sheet membranes with three different substrate structures. After using a RO configuration, the A values were 4.58×10^{-12}, 5.81×10^{-12} and 6.33×10^{-12} m Pa^{-1} s^{-1}, while the B values were 1.86×10^{-7}, 2.42×10^{-7} and 2.22×10^{-7} m s^{-1} and S value were 510, 554 and 687 μm. Han et al. [30] developed a high performance TFC PRO membrane for osmotic power generation. This membrane showed a A value 1.47×10^{-11} m Pa^{-1} s^{-1}, 5.56×10^{-7} m s^{-1} and about 436 μm values for B and S, respectively. Hoover et al. [31] developed a thin film composite membrane with polyethylene terephthalate nanofibers. They A, B and S values of 3.14×10^{-12} m Pa^{-1} s^{-1}, 6.39×10^{-8} m s^{-1} and 651 μm, respectively.

There are three main aspects that should be taken into consideration when full-scale performance estimation of a PRO is carried out; modeling [32], characteristics of membrane elements [33,34] and operating conditions [16,35]. The transport equations used in PRO are quite similar to those used in reverse osmosis (RO) process [36]. The main difference is that in PRO process both internal and external concentration polarization (ICP and ECP, respectively) phenomena are considered (Fig. 1). There are some limitations when a PRO system is scaled-up that should be taken into consideration in the transport equation such as limited membrane surface per element (S_m), element pressure drop (Δp) in the draw side and feed side, dilution of the draw solution (DS) and concentration of the feed solution (FS) along the membrane element, void fraction or porosity (ε) of both, draw side and feed side [37]. Numerical modeling such as computational fluid dynamics (CFD) applied to PRO process [38] can be very useful in order to understand the transport phenomena and improve spacers and membrane characteristics [39–42]. The main problem with these numerical simulations is the high computational time if it would be applied to a

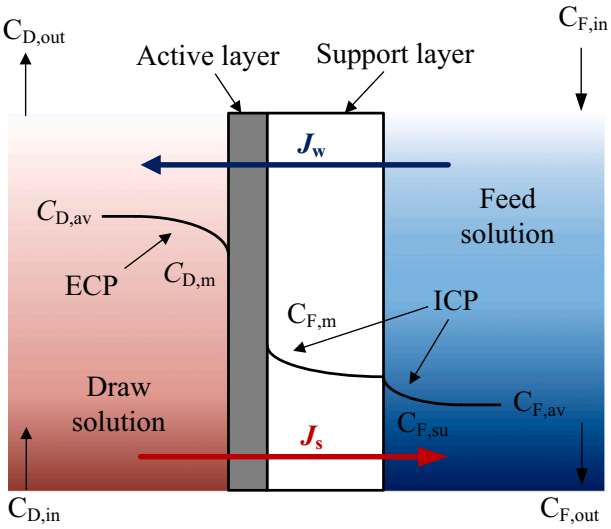

Fig. 1. Concentration profile across the PRO membrane considering ECP and ICP.

full-scale PRO system. Therefore, as with RO system simulators [43], concentrated parameter models instead of distributed parameter models are usually applied. This allows reducing the computational time by considering averages in terms of operating parameters per membrane module. Ruiz-García et al. [16] proposed a computational tool that takes the mentioned factor into consideration for spiral wound membrane modules (SWMMs). In this case, the computational tool estimates the performance of full-scale PRO systems with one stage (up to 8 SWMMs in series in a pressure vessel (PV)) applying averages per membrane module. As it occur in RO systems limiting operating factors in terms of pressure and flows were also considered. Matta et al. [44] also developed a PRO simulator for SWMMs considering a 2D discretization. This simulation was developed for estimating the performance of a single SWMM but, it allows comparing flat sheet membranes with SWMMs. Limitation in terms of operating conditions were not implemented. Touati et al. [45,46] have reported a performance assessment of hybrid RO-PRO processes. These studies did not take into consideration the limitation of having SWMMs in series such as Δp, limiting operating factors in terms of pressure or flows. Salamanca et al. [47] reported an estimation of osmotic power in the Magdalena river but, concerning the PRO system, only a *PD* value of 5 W m^{-2} was used for the study. Taking only the power density value without taking into account other parameters omits many factors of PRO systems that affect the performance of a real PRO plant [16]. Obode et al. [48] carried out a techno-economic study considering full-scale PRO plant, however the impact of disposing membrane element in series on plant performance was not considered. The impact of hydrodynamic conditions on optimum osmotic power generation in a dual-stage PRO system using SWMMs was carried out by Al-Zainati et al. [49]. One of the limitations of this work is the consideration of only two SWMMs in series in the first stage and only 1 in the second stage. Al-Zainati et al. [50] did a performance estimation of multiple stage PRO systems for energy generation. In this study up to 4 stages were considered reaching a *PD* value of 15 W m^{-2} using the data of a HF PRO membrane from Toyobo Co. Ltd. [51]. It was concluded that with more stages the *PD* was higher.

Currently, PRO technology is not viable for the massive generation of electricity [52], which would be produced by mixing seawater with river water. This has led to the study of other alternative uses for PRO technology, such as the design of hybrid systems with other technologies such as RO-PRO [53–55] for reducing the specific energy consumption (*SEC*) of the RO system, PRO-MBR [56], PRO-MD [57], close circuit PRO [58] or its use in very specific fields where hypersaline solutions (60–180 g L^{-1}) are available such as hydrocarbon produced water, hypersaline lakes, salt domes, geothermal water or desalination brine [59–61]. Studying the viability of PRO technology for these applications must take into account the characteristics of the membranes and their modules in full-scale systems. The aim of this study was to assess the effect of the permeability coefficients A and B, S, S_m and $C_{D,in}$ on the performance of a single-stage full-scale PRO process using SWMMs. Optimal operating points considering were also estimated by using a simulation tool for full-scale PRO systems considering boundary conditions and limitations of scaling-up PRO systems to provide estimates as close to operating reality as possible.

2. Material and methods

2.1. Model equations

Performance of PRO processes mainly depends on flows, pressures, concentrations and membrane characteristics. In this study, equations based on fundamental thermodynamics that describe the transport of solvent and solute across a semipermeable membrane were used. These principles elucidate the free energy that is produced during the spontaneous mixing of DS and FS [62,63]. It should be mentioned that the equations used were applied considering averages per SWMM, it means that the inputs in terms of flow (Q), pressure (p), concentration (C), etc. were assumed the same for the entire SWMM. The output parameters of one SWMM were the input parameters of the following SWMM arranged in series in a PV (Fig. 2). Despite this consideration, the Δp along the SWMM on both sides (draw and feed), as well as the concentration of the feed and the dilution of the draw along the SWMM, were taken into account. From the above mentioned theory, it can be deduced that the permeate flux (J_p) is the product of A and the driving force across the membrane [62] (Eq. (1)):

$$J_p = A(\Delta\pi - \Delta p) \tag{1}$$

where $\Delta\pi$ is the osmotic pressure gradient and Δp the pressure gradient, both across the membrane. To obtain Q_p, J_p was multiplied by S_m. To determine $\Delta\pi$, the concentration on the membrane surface on both the draw and feed side has to be estimated. For this purpose, the effect of external and internal concentration polarization (ECP and ICP, respectively) has to be considered (1).

$$A = A_0 \cdot TCF \cdot FF \tag{2}$$

$$\Delta\pi = \pi_{D,m} - \pi_{F,m} \tag{3}$$

$$\pi = 3.805C^2 + 42.527C + 0.434 \tag{4}$$

where A_0 is the initial value of A, TCF the temperature correction factor (value of 1.0 at 25 °C, which is the T considered in this study) [16] and FF the fouling factor (in this study it had the value of 1.0 as membrane without fouling was considered). $\pi_{D,m}$ and $\pi_{F,m}$ are the osmotic pressure on the membrane surface on the draw and feed side, respectively. Eq. (4) [64] was used to calculate osmotic pressure from an NaCl concentration (mol L^{-1}). For the calculation of $\pi_{D,m}$ and $\pi_{F,m}$, $C_{D,m}$ and $C_{F,m}$ were used, respectively, in Eq. (4).

$$C_{D,m} = \left(C_{D,av} + \frac{J_s}{J_p}\right) e^{\frac{-J_p}{k_D}} - \frac{J_s}{J_p} \tag{5}$$

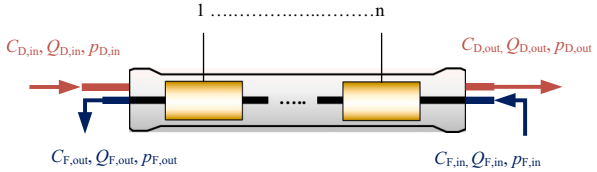

Fig. 2. Flow diagram of single-staged PRO system.

$$C_{F,m} = \left(C_{F,av} + \frac{J_s}{J_p}\right) e^{\frac{J_p}{k_F}} e^{KJ_p} - \frac{J_s}{J_p} \quad (6)$$

$$C_{x,av} = 0.5\left(C_{x,in} + C_{x,out}\right) \quad (7)$$

$$C_{F,av} = 0.5\left(C_{F,in} + C_{F,out}\right) \quad (8)$$

$$J_s = J_p \frac{B}{A\beta RT}\left(1 + \frac{A\Delta p}{J_p}\right) \quad (9)$$

$$k_x = \frac{Sh_x D_{x,av}}{d_{h,x}} \quad (10)$$

where $C_{D,m}$ and $C_{F,m}$ are the concentrations on the membrane surface on the draw and feed sides considering ECP and ICP [65], $C_{D,av}$ and $C_{D,av}$ are the average concentrations on the draw and feed side, J_s the reverse solute flux, k_D and k_F the mass transfer coefficients on the draw and feed side, and $C_{D,in}$ and $C_{D,out}$ are the input and output concentrations on the draw side. β is the dimensionless Van't Hoff factor for strong electrolytes ($\beta = 2$ for NaCl) [64], R is the gas constant (8.31 J mol^{-1} K^{-1}) and T is the absolute temperature (in K) of the solution, taken as 25 °C for both solutions (DS and FS) in this study. It should be noted that the proposed methodology is able to simulate PRO systems with different temperatures by considering T dependent equations for D, ρ and μ. Sh_x is the Sherwood numbers for the draw (dilutive) and feed (concentrative) [66] (x can be the feed or draw side), $D_{x,av}$ is the diffusion coefficient of the x side (using $C_{x,av}$ in Eq. (18), and $d_{h,x}$ is the hydraulic diameters for the x side. Sh is a dimensionless number related with the ratio of convective to diffusive mass transport. Considering a laminar flow regime due to the low cross-flow rate used in this study, Sh_x can be estimated through Eqs. (12) and (13), respectively [66]:

$$K = \frac{S}{D_{F,av}} \quad (11)$$

$$Sh_D = 1.849\left(Re_D Sc_D \frac{d_{h,D}}{L}\right)^{1/3}\left(1.002 - 0.0319\gamma_D + 0.00034\gamma_D^2 - 0.001\gamma_D^3\right) \quad (12)$$

$$Sh_F = 1.849\left(Re_F Sc_F \frac{d_{h,F}}{L}\right)^{1/3}\left(0.997 + 0.315\gamma_F + 0.022\gamma_F^2 - 0.008\gamma_F^3\right) \quad (13)$$

$$\gamma_x = \frac{P_{ew,x}}{\left(Re_x Sc_x \frac{d_{h,x}}{L}\right)^{1/3}} \quad (14)$$

$$P_{ew,x} = \frac{J_p d_{h,x}}{D_x} \quad (15)$$

$$Re_x = \frac{\rho_{x,av} \cdot \nu_{x,av} \cdot d_{h,x}}{\mu_{x,av}} \quad (16)$$

$$Sc_x = \frac{\mu_{x,av}}{\rho_{x,av} \cdot D_x} \quad (17)$$

$$D_{x,av} = -1.025 \times 10^{-10} C + 1.518 \times 10^{-9} \quad (18)$$

$$\rho_{x,av} = -1.047C^2 + 39.462C + 997.370 \quad (19)$$

$$d_{h,x} = \frac{4\varepsilon_x}{\frac{2}{H_x} + (1 - \varepsilon_x)\frac{8}{H_x}} \quad (20)$$

where γ_x, $P_{ew,x}$, Re_x, Sc_x, $\rho_{x,av}$ and $\mu_{x,av}$ are, for each side respectively, a lumped parameter, wall Peclet number, Reynolds number, Schmidt number, solution density and dynamic viscosity. ρ and μ were calculated for each solution (DS and FS) through Eqs. (19) and (21) with $C_{D,av}$ and $C_{F,av}$ in mol L^{-1}.

$$\mu_{x,av} = 0.001\left(0.012C^2 + 0.065C + 0.985\right) \quad (21)$$

The term Δp (Eq. (1)) was calculated considering the pressure drop on both the draw and feed side.

$$\Delta p = p_{D,in} - \frac{PL_D}{2} - p_{F,in} + \frac{PL_F}{2} \quad (22)$$

$$PL_x = \lambda_x \cdot L \cdot \frac{\rho_x}{d_{h,x}} \frac{\nu_{x,av}^2}{2} \quad (23)$$

$$\lambda_x = K_\lambda \cdot 6.23 Re_x^{-0.3} \quad (24)$$

where $p_{D,in}$ and $p_{F,in}$ are the input pressures on the draw and feed side, PL_x is the pressure losses on the x side, L is the length of the membrane module and K_λ a parameter introduced by V. Geraldes et al. [67] to take into consideration additional pressure losses in the feed of the PVs and the SWMM fittings. Due to lack of information, K_λ was assumed to be the same for the draw and feed side. The concentrations in the output on both sides ($C_{D,out}$ and $C_{F,out}$) are affected by Q_p and J_s. The DS is diluted and the FS is concentrated due to both Q_p and J_s. The dilution and concentration factors (DF and CF) due to Q_p are defined in Eqs. (25) and (26) respectively.

$$DF = \frac{C_{D,out}}{C_{D,in}} = \frac{1 - Y_m}{1} \quad (25)$$

$$CF = \frac{C_{F,out}}{C_{F,in}} = \frac{1}{1 - Y_m} \quad (26)$$

where $\underline{C}_{D,out}$ and $\underline{C}_{F,out}$ are the output concentrations due to only Q_p and Y_m is the recovery fraction of the SWMM ($Q_p/Q_{F,in}$). The calculated R is Y_m in percentage. Mass fluxes (in kg s^{-1}) in the DS and FS are shown in Eqs. (27) and (28):

$$C_{D,out}\left(Q_{D,in} + Q_p\right) = C_{D,in} DF\left(Q_{D,in} + Q_p\right) - J_s \quad (27)$$

$$C_{F,out}\left(Q_{F,in} - Q_p\right) = C_{F,in} CF\left(Q_{F,in} - Q_p\right) + J_s \quad (28)$$

2.2. Parameters of the PRO SWMMs and simulation conditions

There is one commercial FO SWMM available (HTI OsMem™ 2521 [68]) that has been tested under PRO conditions. The characteristics of the mentioned FO SWMM were chosen as it was done in a previous study of the author [18]. This SWMM was up-scaled to an 8 in like in a previous study [18]. Information about the porosity parameters (as unit fraction) of both, draw (ε_D) and feed (ε_F) sides are not available for the mentioned SWMM so, the values from a previous published study [69] for RO SWMMs were used. Some parameters of the PRO SWMM (Table 1) were taken from [68]. Table 1 shows the considered ranges of $C_{D,in}$, A, B and S considering the data available in the literature for flat sheet membranes. Limiting rejection flow in both sides were established as it happens in RO systems. The operating range was between 2 and 16 m^3 h^{-1}, it means that all operating points that were out of the mentioned range were dismissed. Limitations in terms of maximum flux recovery and permeate flow per SWMM were not established. All calculations were made considering a PV of up to 8 SWMMs, so more PVs in parallel would be necessary to generate more P.

2.3. Performance assessment

To estimate the net energy that can be generated from a single-staged

Table 1
Parameters of the used 8-inch PRO SWMM and operating ranges.

Parameter	Range or value
A (m Pa^{-1} s^{-1})	2.65×10^{-12}–1.06×10^{-11}
B (m s^{-1})	1.22×10^{-7}–6.11×10^{-7}
S_m (m^2)	15.53, 25.53, 35.53
S (μm)	135, 446, 757
L (m)	1.0
H_D (m)	1.1×10^{-3}
H_F (m)	1.5×10^{-3}
ε_D	0.89
ε_F	0.65
FF	1
T (°C)	25
$C_{D,in}$ (g L^{-1})	60–180
$Q_{D,in}$ (m^3 h^{-1})	3–16
$p_{D,in}$ (MPa)	0.5–9.5
$C_{F,in}$ = (g L^{-1})	0.5
$Q_{F,in}$ (m^3 h^{-1})	3–16
$p_{F,in}$ (MPa)	0.2

full-scale PRO system, it was necessary to know the specific enthalpy (h) in the hydraulic turbine input and output as well as in the pumps as this process includes devices such as draw and feed pump, an energy recovery device (pressure exchanger and booster pump) and turbine Fig. 3. The power (P) of these devices was considered in this study. Eqs. (29)–(31) were used to calculated h [70]. For non-atmospheric pressures (p_0), specific enthalpy ($h(T,p,C)$) was estimated using Eq. (31). From the PRO system results, the power in the hydraulic turbine (P_{TB}), draw, booster and feed pumps ($P_{pump,draw}$, $P_{pump,boost}$ and $P_{pump,feed}$, respectively) were calculated using Eqs. (32)–(39). The net power (P_{net}) was determined using Eq. (40). The output pressure of the draw pump (input of pressure exchanger) was 0.5 bar.

$$h(T,p_0,C) = h_w - C\left(b_1 + b_2 w_s + b_3 w_s^2 + b_4 w_s^3 + b_5 T + b_6 T^2 + b_7 T^3 + b_8 w_s T + b_9 w_s^2 T + b_{10} w_s T^2\right) \quad (29)$$

$$h_w = 141.355 + 4202.070T - 0.535T^2 + 0.004T^3 \quad (30)$$

$$b_1 = -2.348 \times 10^4,\ b_2 = 3.152 \times 10^5,\ b_3 = 2.803 \times 10^6,$$
$$b_4 = -1.446 \times 10^7,\ b_5 = 7.826 \times 10^3,\ b_6 = -4.417 \times 10^1,$$
$$b_7 = 2.139 \times 10^{-1},\ b_8 = -1.991 \times 10^4,\ b_9 = 2.778 \times 10^4,$$
$$b_{10} = 9.728 \times 10^1$$

$$h(T,p,C) = h(T,p_0,C) + \vartheta(p - p_0) \quad (31)$$

where ϑ is the specific volume (the inverse of ρ). ϑ was determined for both the DS and FS using ρ of DS and FS in the input and output of the different devices.

$$P_{TB} = \eta_{TB}\dot{m}_{TB}\left(h_{TB,in} - h_{TB,out}\right) \quad (32)$$

$$\dot{m}_{TB} = Q_p \cdot \rho_{D,out} \quad (33)$$

$$P_{pump,draw} = \frac{\dot{m}_{pump,draw}\left(h_{pump,draw,in} - h_{pump,draw,out}\right)}{\eta_{pump,draw}} \quad (34)$$

$$\dot{m}_{pump,draw} = Q_{D,in} \cdot \rho_{D,in} \quad (35)$$

$$P_{pump,boost} = \frac{\dot{m}_{pump,boost}\left(h_{pump,boost,in} - h_{pump,boost,out}\right)}{\eta_{pump,boost}} \quad (36)$$

$$\dot{m}_{pump,boost} = Q_{D,in} \cdot \rho_{D,in} \quad (37)$$

$$P_{pump,feed} = \frac{\dot{m}_{pump,feed}\left(h_{pump,feed,in} - h_{pump,feed,out}\right)}{\eta_{pump,feed}} \quad (38)$$

$$\dot{m}_{pump,feed} = Q_{F,in} \cdot \rho_{F,in} \quad (39)$$

$$P_{net} = P_{TB} - P_{pump,draw} - P_{pump,boost} - P_{pump,feed} \quad (40)$$

$$PD_{net} = \frac{P_{net}}{nS_m} \quad (41)$$

where η_{TB} is the efficiency of the turbine (assumed as 85 %), η of the three pumps were assumed as 80 % and n the number of SWMMs in the PRO system.

3. Results and discussion

This section is divided into five sub-sections where the impact of the different parameters studied ($C_{D,in}$, A, B, S_m and S) on the performance of full-scale PRO system was analyzed considering a single stage.

3.1. Influence of $C_{D,in}$

Fig. 4 shows the increase of $PD_{net,max}$ with the SWMMs in series and $C_{D,in}$. The highest values were achieved with 8 SWMMs in series and this was because this was the maximum number of elements considered due to the fact that only single-stage PRO systems were evaluated. This trend held for all A and B values considered in this study. This suggests that higher $PD_{net,max}$ could be obtained with systems with more than one stage [50] but, it should be considered limiting operating conditions such as maximum flow in DS and FS as well as minimum flow also in both side, this could limit the number of stages. Considering the energy consumption of the pumps showed the difference in terms of $PD_{net,max}$ in comparison with a previous study by the authors in which only the hydraulic turbine was considered. In the mentioned study, PD_{max} were

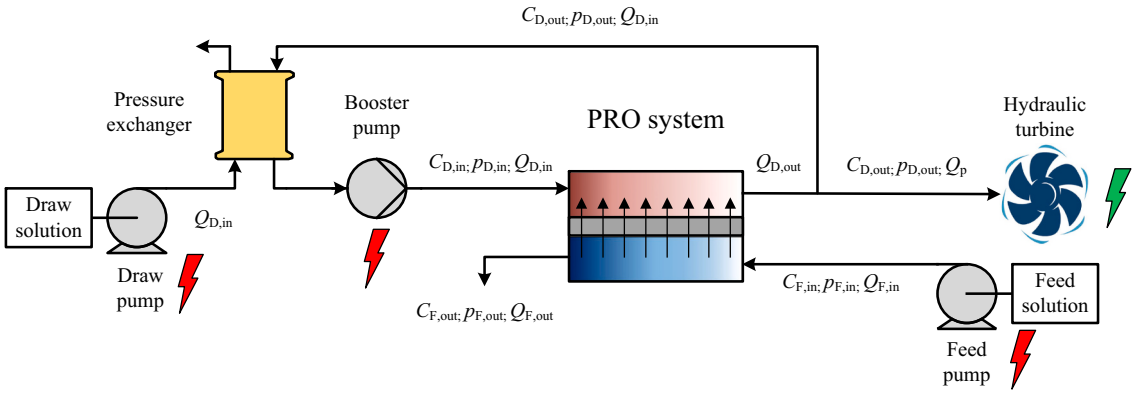

Fig. 3. Flow diagram of the PRO plant.

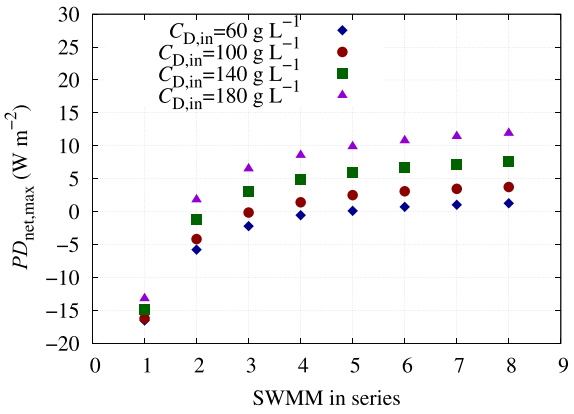

Fig. 4. $PD_{net,max}$ (kW) for different values of $C_{D,in}$, $A = 5.3 \times 10^{-12}$ m Pa^{-1} s^{-1}, $B = 2.04 \times 10^{-7}$ m s^{-1}, $S_m = 15.53$ m^2, $S = 446$ μm and considering from 1 to 8 SWMMs in series.

obtained with 3 SWMMs in series [16]. As the highest $PD_{net,max}$ vales were obtained with 8 SWMMs in series means that $P_{net,max}$ was also determined with the same number of SWMMs in series, therefore, the next results to be shown will be considering the maximum number of SWMMs in series, 8.

Fig. 5 shows P for the devices considered and for the operating point that maximize P_{net} with $S_m = 15.53$ m^2, $A = 5.3 \times 10^{-12}$ m Pa^{-1} s^{-1}, $B = 2.04 \times 10^{-7}$ m s^{-1} and 8 SWMMs in series. Percentage-wise, the higher the Cd, the lower the percentage of P consumed by the pumps. For $C_{D,in}$ = 80 g L^{-1}, the P_{TB} was 762.7 W while for $C_{D,in} = 180$ g L^{-1} it was 2394 W. Considering the $P_{net,max}$ and 8 SWMMs in series, a specific energy generation of 0.28 and 0.37 kWh m^{-3} was obtained for $C_{D,in}$ of 80 and 180 g L^{-1}, respectively. As $\Delta\pi$ considering both sides of the membrane decreases, the consumption of the pumps increases in percentage terms with respect to the P_{TB}, which makes the window of operating points that provide a positive P_{net} increasingly narrower.

3.2. Influence of A

Fig. 6 the $P_{net,max}$ variation with the increase of A and $C_{D,in}$ ($P_{net,max}$ was obtaining with 8 SWMMs in series). As it was expected, $P_{net,max}$ increase with A and $C_{D,in}$. For high A values, $C_{D,in}$ had more impact on $P_{net,max}$ than for low A values. This can be observed in Tables 2 and 3. From Table 2 it can be seen how the value of $P_{net,max}$ went from 25.57 to 1418.13 W considering $C_{D,in}$ = 60 and 180 g L^{-1} respectively. However, for the same $C_{D,in}$ values, and considering a value of A three times higher

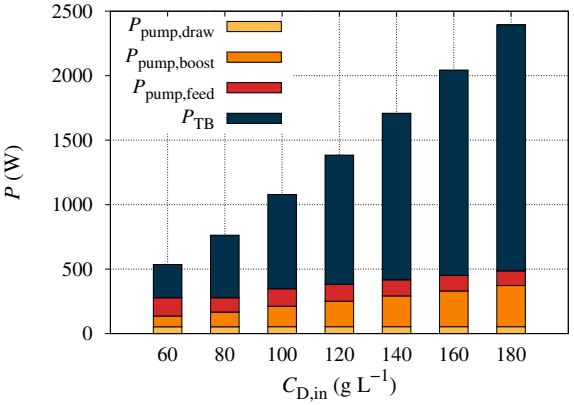

Fig. 5. P (W) values for the different devices and $C_{D,in}$ for the operating points that maximize P_{net} considering $S_m = 15.53$ m^2, $A = 5.3 \times 10^{-12}$ m Pa^{-1} s^{-1}, $B = 2.04 \times 10^{-7}$ m s^{-1}, $S = 446$ μm and 8 SWMMs in series.

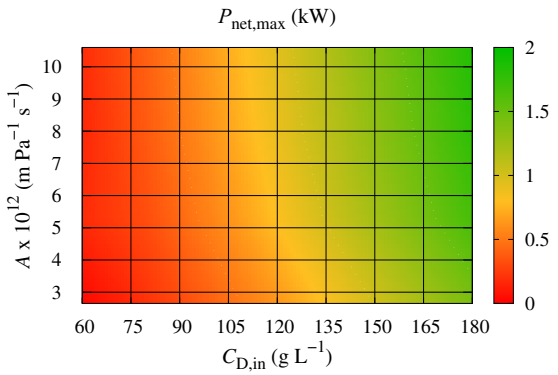

Fig. 6. $P_{net,max}$ (kW) for different values of A and $C_{D,in}$ with $B = 1.22 \times 10^{-7}$ m s^{-1}, $S = 446$ μm, 8 SWMMs in series and $S_m = 15.53$ m^2.

than in the previous case, $P_{net,max}$ went from 155.33 to 1777.33 W, showing a higher increase in the latter case. It can also be seen from Fig. 6, how a certain point is reached at which the increases in A are losing impact on the increases in $P_{net,max}$ for a given $C_{D,in}$ and B values. In fact, the $P_{net,max}$ values obtained for $C_{D,in}$ = 60 g L^{-1}, $B = 1.22 \times 10^{-7}$ m s^{-1} and A values of 2.65×10^{-12}, 5.3×10^{-12}, 7.95×10^{-12} and 1.06×10^{-11} m Pa^{-1} s^{-1} were 25.57, 119.49, 155.33 and 180.67 W respectively, which shows a decay in the increases of $P_{net,max}$. In terms of optimal operating parameters, from Table 2 it can be seen that the higher was $C_{D,in}$ the higher was $p_{D,in}$, $Q_{F,in}$ and R for getting the max value of P_{net}. Increasing the coefficient A had an impact on the optimal operating parameters, lower $p_{D,in}$ and R but, higher $Q_{F,in}$. From the results it can be seen how the operating points obtained by the author in previous studies [16,18] to maximize the P generated in the turbine without taking into account the energy consumption of the pumps and their efficiency differ considerably if the pumps are taken into account. The mentioned previous studies established high values of $Q_{D,in}$ to maximize P_{TB}, however, it can be seen how, taking into account the pumps, the value of $Q_{D,in}$ that maximizes P_{net} is the minimum considered (3 m^3 h^{-1}). This is because there were two pumps that had to boost $Q_{D,in}$, the draw and booster pumps. The $p_{D,in}$ value that maximized P_{net} depends also on the A coefficient. For $C_{D,in}$ solutions between 120 and 180 g L^{-1}, the higher the A coefficient the slightly lower the $p_{D,in}$ that maximized $P_{net,max}$ (Tables 2 and 3).

3.3. Influence of B

Fig. 7 shows the calculated $P_{net,max}$ considering ranges of B and $C_{D,in}$. The increase of coefficient B made $P_{net,max}$ to decrease for a constant $C_{D,in}$ value to the increase of reverse solute flux. This can happen in the operation of PRO systems, as one of the possible effects of fouling is the increase of the coefficient B. Comparing Tables 3 and 4 it can be seen that the decrements of $P_{net,max}$ due to the increase of coefficient B. The decreases in $P_{net,max}$ due to the increase in B increase as $C_{D,in}$ increases. For $C_{D,in}$ = 60 g L^{-1} a difference of 147.44 W was observed, whereas for $C_{D,in}$ = 120 g L^{-1} the difference was 351.52 W. The increase of B also influenced the optimal operating parameters. As B increased, $p_{D,in}$ that maximized P_{net} was lower as well as R (Tables 3 and 4).

3.4. Comparison between the influence of A and B

Table 5 shows how $P_{net,max}$ was varied with the variation of coefficients A and B. The variation of these coefficient do not only allow a performance analysis considering different SWMMs but also how hypothetical fouling conditions where coefficient A decreases and/or coefficient B increases would affect $P_{net,max}$. An A decrease from 1.06×10^{-11} to 7.95×10^{-12} m Pa^{-1} s^{-1} and $B = 1.22 \times 10^{-7}$ m s^{-1}

Table 2
Operating points for $P_{net,max}$ with $S_m = 15.53\ m^2$, $S = 446\ \mu m$ and 8 SWMMs in series for different values of $C_{D,in}$, $B = 1.22 \times 10^{-7}\ m\ s^{-1}$ and $A = 2.65 \times 10^{-12}\ m\ Pa^{-1}\ s^{-1}$.

Parameter	$C_{D,in}$ (g L^{-1})						
	60	80	100	120	140	160	180
$p_{D,in}$ (MPa)	1.95	2.6	3.25	4	4.7	5.4	6.15
$Q_{D,in}$ ($m^3\ h^{-1}$)	3	3	3	3	3	3	3
$Q_{F,in}$ ($m^3\ h^{-1}$)	3.5	3.5	4	5	5.5	6	6.5
R (%)	19.15	25.62	32.07	39.53	46.49	53.46	60.94
$P_{net,max}$ (W)	25.57	204.81	401.70	625.52	873.37	1138.64	1418.13

Table 3
Operating points for $P_{net,max}$ with $S_m = 15.53\ m^2$, $S = 446\ \mu m$ and 8 SWMMs in series for different values of $C_{D,in}$, $B = 1.22 \times 10^{-7}\ m\ s^{-1}$ and $A = 7.95 \times 10^{-12}\ m\ Pa^{-1}\ s^{-1}$.

Parameter	$C_{D,in}$ (g L^{-1})						
	60	80	100	120	140	160	180
$p_{D,in}$ (MPa)	1.95	2.6	3.25	3.9	4.6	5.25	6
$Q_{D,in}$ ($m^3\ h^{-1}$)	3	3	3	3	3	3	3
$Q_{F,in}$ ($m^3\ h^{-1}$)	4	4.5	5	6	6.5	7	7.5
R (%)	19.09	25.53	31.98	38.42	45.37	51.83	59.31
$P_{net,max}$ (W)	155.33	374.20	619.05	887.39	1171.92	1469.24	1777.33

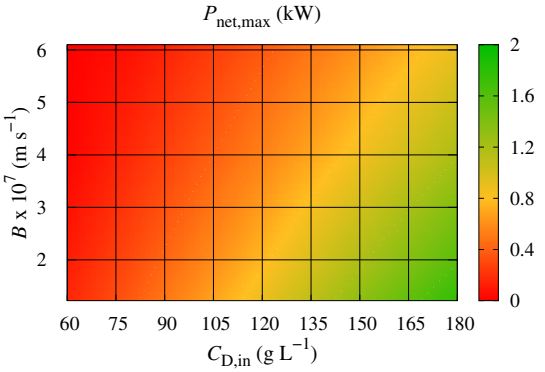

Fig. 7. $P_{net,max}$ (kW) for different values of B and $C_{D,in}$ with $A = 7.95 \times 10^{-12}$ m $Pa^{-1}\ s^{-1}$, $S = 446\ \mu m$, 8 SWMMs in series and $S_m = 15.53\ m^2$.

produced a $P_{net,max}$ decrease of 68.76 W however, for the same A decrease, the $P_{net,max}$ decrease was not the same for the different B values, being 67.47, 62.75 and 57.04 W for $B = 2.04 \times 10^{-7}$, 4.06×10^{-7} and $6.10 \times 10^{-7}\ m\ s^{-1}$, respectively. So, the higher was B value the lower impact had A decrease on $P_{net,max}$. However, for different A values, decrements in terms of B had fairly similar impacts on $P_{net,max}$.

3.5. Influence of S_m

Fig. 8 shows the impact of the SWMMs in series and S_m on $P_{net,max}$. It can be seen that the higher is S_m the higher was $P_{net,max}$ and the differences in terms of $P_{net,max}$ between S_m were higher with more SWMMs in series. The difference between considering S_m of 15.53 and 35.53 m^2 was 376.77 W for 3 SWMMs in series while for 8 SWMMs in series it was 1027.42 W. The increment of S_m had also impact on the optimal operating parameters making the optimal conditions to change. The increase of S_m made $Q_{D,in}$ and $Q_{D,in}$ to increase for maximizing P_{net} however, R and $p_{D,in}$ were broadly similar for all three cases (Table 6). The higher the $C_{D,in}$, the greater the difference between the $P_{net,max}$ obtained for different S_m (Fig. 9). Considering S_m of 15.53 and 35.53 m^2 (And the A and B values of 7.95×10^{-12} m $Pa^{-1}\ s^{-1}$ and 2.04×10^{-7} m s^{-1}, respectively), the difference for 60 g L^{-1} was 332.85 W, while for 140 g L^{-1} it was 1415.70 W, so that at higher $C_{D,in}$ the S_m parameter has more impact on $P_{net,max}$.

3.6. Influence of S

Table 7 shows the impact of the parameter S on $P_{net,max}$ for two different $C_{D,in}$ (60 and 160 g L^{-1}) and also its impact on the optimal

Table 5
$P_{net,max}$ (W) for different A and B values, 8 SWMMs in series, $C_{D,in} = 60\ g\ L^{-1}$, and $S_m = 35.53\ m^2$.

$A \times 10^{-12}$	$B \times 10^{-7}$ (m s^{-1})			
(m $Pa^{-1}\ s^{-1}$)	1.22	2.04	4.06	6.10
2.65	307.50	241.13	108.37	55.49
5.30	459.43	376.30	214.31	88.09
7.95	535.24	443.00	263.15	120.68
10.6	580.73	482.44	288.52	153.28

Table 4
Operating points for $P_{net,max}$ with $S_m = 15.53\ m^2$, $S = 446\ \mu m$ and 8 SWMMs in series for different values of $C_{D,in}$, $B = 4.06 \times 10^{-7}\ m\ s^{-1}$ and $A = 7.95 \times 10^{-12}\ m\ Pa^{-1}\ s^{-1}$.

Parameter	$C_{D,in}$ (g L^{-1})						
	60	80	100	120	140	160	180
$p_{D,in}$ (MPa)	1.65	2.05	2.75	3.3	3.95	4.55	5.2
$Q_{D,in}$ ($m^3\ h^{-1}$)	3	3	3	3	3	3	3
$Q_{F,in}$ ($m^3\ h^{-1}$)	4.5	4.5	5	5.5	6.5	7	7.5
R (%)	16.01	19.95	26.86	32.28	38.69	44.61	51.03
$P_{net,max}$ (W)	7.89	173.08	347.46	535.87	739.86	955.51	1180.94

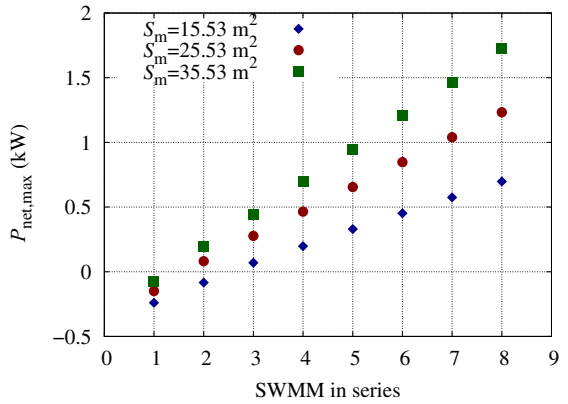

Fig. 8. $P_{net,max}$ (kW) for different values of S_m, $A = 5.3 \times 10^{-12}$ m Pa^{-1} s^{-1}, $B = 2.04 \times 10^{-7}$ m s^{-1}, $C_{D,in} = 120$ g L^{-1}, $S = 446$ μm and considering from 1 to 8 SWMMs in series.

Table 6
Operating points for $P_{net,max}$ for different S_m values, $S = 446$ μm, 8 SWMMs in series, $C_{D,in} = 120$ g L^{-1}, $B = 2.04 \times 10^{-7}$ m s^{-1} and $A = 5.3 \times 10^{-12}$ m Pa^{-1} s^{-1}.

Parameter	S_m (m^2)		
	15.53	25.53	35.53
$p_{D,in}$ (MPa)	37.5	38	38
$Q_{D,in}$ (m^3 h^{-1})	3.0	3	3.5
$Q_{F,in}$ (m^3 h^{-1})	5.5	8.5	11.5
R (%)	36.93	37.65	37.70
$P_{net,max}$ (W)	697.77	1233.20	1725.19

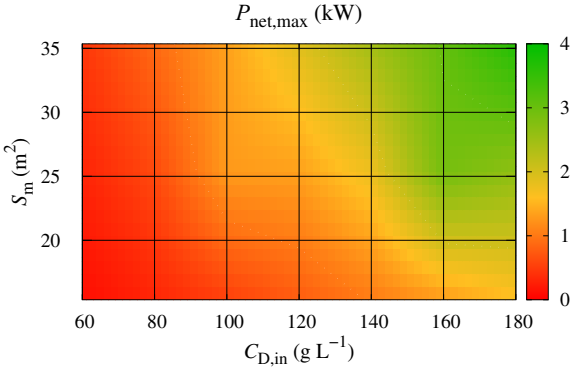

Fig. 9. $P_{net,max}$ (kW) for different values of S_m and $C_{D,in}$, $A = 7.95 \times 10^{-12}$ m Pa^{-1} s^{-1}, $B = 2.04 \times 10^{-7}$ m s^{-1}, $S = 446$ μm and 8 SWMMs in series.

operating parameters. An increase in S from 135 to 757 μm produced a decrease in $P_{net,max}$ of 62 % for $C_{D,in}$ of 60 g L^{-1} and 33 % for $C_{D,in}$ of 160 g L^{-1}. This indicates that at higher $C_{D,in}$ the impact of the S parameter on $P_{net,max}$ decreases. An increment of S produced slightly decrements on R in the optimal operating point for $C_{D,in} = 60$ g L^{-1}. For $C_{D,in} = 160$ g L^{-1}, increments of Sresulted in optimal operating points being obtained at higher R and slightly higher $p_{D,in}$. It should be noted that the $C_{F,in}$ considered in this study was low (0.5 g L^{-1}), it is possible that the impact of the parameter S also varies with different $C_{F,in}$ values.

From the results it can be observed that the $p_{D,in}$ value that maximized $P_{net,max}$ and $PD_{net,max}$ depends on characteristics of the SWMM such as A, B, S_m and S (Tables 2, 3, 4 and 7). In addition to this, it depends on the number of SWMMs in series (Fig. 4) and certainly on the number of stages considered. Therefore, considering that the value of $p_{D,in}$ that maximizes $PD_{net,max}$ is $\Delta\pi/2$ is not accurate. In fact, the relation

Table 7
Operating points for $P_{net,max}$ for different S values, $S_m = 15.53$ m^2, 8 SWMMs in series, $C_{D,in} = 60$ and 160 g L^{-1}, $B = 1.22 \times 10^{-7}$ m s^{-1} and $A = 5.3 \times 10^{-12}$ m Pa^{-1} s^{-1}.

Parameter	$C_{D,in}$ (g L^{-1})					
	60			160		
	S (μm)					
	135	446	757	135	446	757
$p_{D,in}$ (MPa)	2.1	1.95	1.95	5.2	5.3	5.5
$Q_{D,in}$ (m^3 h^{-1})	3	3	3	3	3	3
$Q_{F,in}$ (m^3 h^{-1})	3.5	3.5	3.5	7	6.5	6
R (%)	20.61	19.12	19.13	51.35	52.39	54.43
$P_{net,max}$ (W)	163.38	119.49	62.06	1604.28	1370.53	1073.40

between $\Delta\pi$ and $p_{D,in}$and without considering the concentration polarization phenomena and 8 SWMMs in series, $S_m = 35.53$ m^2, $B = 2.04 \times 10^{-7}$ m s^{-1} and $A = 5.3 \times 10^{-12}$ m Pa^{-1} s^{-1} would be between 1.3 and 1.5 (for $C_{D,in} = 60$–180 g L^{-1}) instead of 2 as considered in other studies [50,71]. This relation depends on the operating conditions and the characteristics of the SWMM in terms of A, B, S_m, S, etc. The $PD_{net,max}$ value is useful when comparing the performance of different PRO membranes on a laboratory scale. However, when estimating full-Scale PRO system performance it is not appropriate because it would not be a realistic value. As it can be seen from the results obtained, the $PD_{net,max}$ value varies with the operating conditions and the above-mentioned characteristics of the SWMM (Figs. 4 and 9).

4. Conclusions

In this study we have analyzed the operating points of PRO systems with one stage and up to 8 SWMMs in series that maximize energy production for different values of $C_{D,in}$, A, B, S_m and S. Taking into account the characteristics of the membranes and the transport equations considered, it is concluded that the S parameter has a relevant influence on the performance of single-staged full-scale PRO systems. This influence was shown to be $C_{D,in}$ dependent. Percentage increases in S_m produce close to the same increases in $P_{net,max}$ for the same $C_{D,in}$. In proportional terms, an increase in the coefficient B has more impact than the same increase in the coefficient A, although it is true that the impact of A on $P_{net,max}$ decreases as $C_{D,in}$ increases. However, the impact of B on $P_{net,max}$ keeps quite constant with the increase of $C_{D,in}$. It should be note that the impact of A is limited by flux restrictions. The parameter S has higher impact than A on $P_{net,max}$ at high $C_{D,in}$ values, although B has higher impact than S on $P_{net,max}$ for the studied range of $C_{D,in}$. Taking into account the considerations made in this study, full-scale PRO systems with one stage and SWMMs would be energetically feasible for concentration gradients in the range of 60 to 180 g L^{-1} and for the membrane characteristics considered. Taking the PD as a value to carry out studies considering full-scale PRO systems is not precise, since this value varies with the number of SWMMs in series since it is affected by the evolution of the operating parameters along the PV. The results in terms of $P_{net,max}$ may be compromised by the need for pre-treatment of the feed water, which would require the feed pump to provide a higher pressure than considered in this study. This would be an aspect to be addressed in future studies. The fabrication of full-scale SWMMs and their experimental validation is still necessary to approach the validation of the results obtained and the construction of osmotic gradient power plants. It is also necessary to evaluate the consideration of multi-stage PRO systems that could possibly increase the energy that can be generated.

CRediT authorship contribution statement

A. Ruiz-García: Writing – review & editing, Writing – original draft, Validation, Supervision, Resources, Methodology, Investigation,

Funding acquisition, Formal analysis, Conceptualization.

Declaration of competing interest

The authors declare that they have no known competing financial interests or personal relationships that could have appeared to influence the work reported in this paper.

Data availability

No data was used for the research described in the article.

Acknowledgements

This research is part of the project PID2022-138389OB-C32, funded by MCIN/AEI/10.13039/501100011033/FEDER, EU.

References

[1] A. Rahman, O. Farrok, M.M. Haque, Environmental impact of renewable energy source based electrical power plants: solar, wind, hydroelectric, biomass, geothermal, tidal, ocean, and osmotic, Renew. Sust. Energ. Rev. 161 (2022) 112279, https://doi.org/10.1016/j.rser.2022.112279. URL, https://www.sciencedirect.com/science/article/pii/S136403212200199X.

[2] G.N. Psarros, S.A. Papathanassiou, Generation scheduling in island systems with variable renewable energy sources: a literature review, Renew. Energy 205 (2023) 1105–1124, https://doi.org/10.1016/j.renene.2023.01.099. URL, https://www.sciencedirect.com/science/article/pii/S0960148123001088.

[3] T. Xu, W. Gao, F. Qian, Y. Li, The implementation limitation of variable renewable energies and its impacts on the public power grid, Energy 239 (2022) 121992, https://doi.org/10.1016/j.energy.2021.121992. URL, https://www.sciencedirect.com/science/article/pii/S0360544221022404.

[4] M. Rastgar, K. Moradi, C. Burroughs, A. Hemmati, E. Hoek, M. Sadrzadeh, Harvesting blue energy based on salinity and temperature gradient: challenges, solutions, and opportunities, Chem. Rev. 123 (16) (2023) 10156–10205, pMID: 37523591. arXiv:https://doi.org/https://doi.org/10.1021/acs.chemrev.3c00168.

[5] R. Rath, D. Dutta, R. Kamesh, M.H. Sharqawy, S. Moulik, A. Roy, Rational design of high power density "Blue Energy Harvester" pressure retarded osmosis (PRO) membranes using artificial intelligence-based modeling and optimization, Energy Convers. Manag. 253 (2022) 115160, https://doi.org/10.1016/j.enconman.2021.115160. URL, https://www.sciencedirect.com/science/article/pii/S0196890421013364.

[6] S.N. Rahman, H. Saleem, S.J. Zaidi, Progress in membranes for pressure retarded osmosis application, Desalination 549 (2023) 116347, https://doi.org/10.1016/j.desal.2022.116347. URL, https://www.sciencedirect.com/science/article/pii/S0011916422008025.

[7] L. Mendoza-Zapata, A. Maturana-Córdoba, R. Mejía-Marchena, A. Cala, J. Soto-Verjel, S. Villamizar, Unlocking synergies between seawater desalination and saline gradient energy: assessing the environmental and economic benefits for dual water and energy production, Appl. Energy 351 (2023) 121876, https://doi.org/10.1016/j.apenergy.2023.121876. URL, https://www.sciencedirect.com/science/article/pii/S0306261923012400.

[8] N. AlZainati, H. Saleem, A. Altaee, S.J. Zaidi, M. Mohsen, A. Hawari, G.J. Millar, Pressure retarded osmosis: advancement, challenges and potential, J. Water Process Eng. 40 (2021) 101950, https://doi.org/10.1016/j.jwpe.2021.101950. URL, https://www.sciencedirect.com/science/article/pii/S2214714421000374.

[9] J. Jang, Y. Kang, J.-H. Han, K. Jang, C.-M. Kim, I.S. Kim, Developments and future prospects of reverse electrodialysis for salinity gradient power generation: influence of ion exchange membranes and electrodes, Desalination 491 (2020) 114540, https://doi.org/10.1016/j.desal.2020.114540. URL, https://www.sciencedirect.com/science/article/pii/S0011916420306615.

[10] E. Altıok, T.Z. Kaya, K. Smolinska-Kempisty, E. Güler, N. Kabay, B. Tomaszewska, M. Bryjak, Salinity gradient energy conversion by custom-made interpolymer ion exchange membranes utilized in reverse electrodialysis system, J. Environ. Chem. Eng. 11 (2) (2023) 109386, https://doi.org/10.1016/j.jece.2023.109386. URL, https://www.sciencedirect.com/science/article/pii/S2213343723001252.

[11] K. Moradi, M. Rastgar, P. Karami, A. Yousefi, S. Noamani, A. Hemmati, M. Sadrzadeh, Performance analysis of the thermo osmotic energy conversion (TOEC) process for harvesting low-grade heat, Chem. Eng. J. Adv. 16 (2023) 100558, https://doi.org/10.1016/j.ceja.2023.100558. URL, https://www.sciencedirect.com/science/article/pii/S2666821123001151.

[12] A.P. Straub, M. Elimelech, Energy efficiency and performance limiting effects in thermo-osmotic energy conversion from low-grade heat, Environ. Sci. Technol. 51 (21) (2017) 12925–12937, pMID: 29022347. arXiv:https://doi.org/https://doi.org/10.1021/acs.est.7b02213, https://doi.org/10.1021/acs.est.7b02213. URL, https://doi.org/10.1021/acs.est.7b02213.

[13] N.Y. Yip, M. Elimelech, Comparison of energy efficiency and power density in pressure retarded osmosis and reverse electrodialysis, Environ. Sci. Technol. 48 (18) (2014) 11002–11012, pMID: 25157687. arXiv:https://doi.org/https://doi.org/10.1021/es5029316.

[14] J.W. Post, J. Veerman, H.V. Hamelers, G.J. Euverink, S.J. Metz, K. Nymeijer, C. J. Buisman, Salinity-gradient power: evaluation of pressure-retarded osmosis and reverse electrodialysis, J. Membr. Sci. 288 (1) (2007) 218–230, https://doi.org/10.1016/j.memsci.2006.11.018. URL, https://www.sciencedirect.com/science/article/pii/S0376738806007575.

[15] M. Sharma, P.P. Das, A. Chakraborty, M.K. Purkait, Clean energy from salinity gradients using pressure retarded osmosis and reverse electrodialysis: a review, Sustain. Energy Technol. Assess. 49 (2022) 101687, https://doi.org/10.1016/j.seta.2021.101687. URL, https://www.sciencedirect.com/science/article/pii/S2213138821007013.

[16] A. Ruiz-García, F. Tadeo, I. Nuez, Simulation tool for full-scale PRO systems using SWMMs, Desalination 541 (2022) 116025, https://doi.org/10.1016/j.desal.2022.116025. URL, https://www.sciencedirect.com/science/article/pii/S0011916422004805.

[17] M. Essalhi, A. Halil Avci, F. Lipnizki, N. Tavajohi, The potential of salinity gradient energy based on natural and anthropogenic resources in Sweden, Renew. Energy 215 (2023) 118984, https://doi.org/10.1016/j.renene.2023.118984. URL, https://www.sciencedirect.com/science/article/pii/S096014812300890X.

[18] A. Ruiz-García, F. Tadeo, I. Nuez, Role of permeability coefficients in salinity gradient energy generation by PRO systems with spiral wound membrane modules, Renew. Energy 215 (2023) 118954, https://doi.org/10.1016/j.renene.2023.118954. URL, https://www.sciencedirect.com/science/article/pii/S0960148123008601.

[19] Q. She, R. Wang, A.G. Fane, C.Y. Tang, Membrane fouling in osmotically driven membrane processes: a review, J. Membr. Sci. 499 (2016) 201–233, https://doi.org/10.1016/j.memsci.2015.10.040. URL, https://www.sciencedirect.com/science/article/pii/S0376738815302702.

[20] A. Cala, A. Maturana-Córdoba, J. Soto-Verjel, Exploring the pretreatments' influence on pressure reverse osmosis: PRISMA review, Renew. Sust. Energ. Rev. 188 (2023) 113866, https://doi.org/10.1016/j.rser.2023.113866. URL, https://www.sciencedirect.com/science/article/pii/S1364032123007244.

[21] L. Wang, X. Lu, N. Guo, X. Cheng, J. Liu, W. Huang, Y. Jin, L. Zhang, L. Zhao, J. Zhang, H. Chu, B. Dong, D. Wu, F. Chen, Fulvic and alginic acid separation during pressure retarded osmosis: governing effects and fouling mechanisms, Sep. Purif. Technol. 306 (2023) 122692, https://doi.org/10.1016/j.seppur.2022.122692. URL, https://www.sciencedirect.com/science/article/pii/S1383586622022493.

[22] T. Yang, T.-S. Chung, Novel thin-film nanocomposite hollow fiber membranes in modules with reduced reverse solute flux for pressure retarded osmosis, Chem. Eng. J. 450 (2022) 138338, https://doi.org/10.1016/j.cej.2022.138338. URL, https://www.sciencedirect.com/science/article/pii/S1385894722038219.

[23] D.L. Zhao, T.-S. Chung, Applications of carbon quantum dots (CQDs) in membrane technologies: a review, Water Res. 147 (2018) 43–49, https://doi.org/10.1016/j.watres.2018.09.040. URL, https://www.sciencedirect.com/science/article/pii/S0043135418307553.

[24] R.R. Gonzales, M.J. Park, T.-H. Bae, Y. Yang, A. Abdel-Wahab, S. Phuntsho, H. K. Shon, Melamine-based covalent organic framework-incorporated thin film nanocomposite membrane for enhanced osmotic power generation, Desalination 459 (2019) 10–19, https://doi.org/10.1016/j.desal.2019.02.013. URL, https://www.sciencedirect.com/science/article/pii/S0011916418324457.

[25] Q. She, D. Hou, J. Liu, K.H. Tan, C.Y. Tang, Effect of feed spacer induced membrane deformation on the performance of pressure retarded osmosis (pro): implications for pro process operation, J. Membr. Sci. 445 (2013) 170–182, https://doi.org/10.1016/j.memsci.2013.05.061. URL, https://www.sciencedirect.com/science/article/pii/S0376738813004924.

[26] X. Song, Z. Liu, D.D. Sun, Energy recovery from concentrated seawater brine by thin-film nanofiber composite pressure retarded osmosis membranes with high power density, Energy Environ. Sci. 6 (4) (2013) 1199–1210.

[27] N.-N. Bui, J.R. McCutcheon, Nanofiber supported thin-film composite membrane for pressure-retarded osmosis, Environ. Sci. Technol. 48 (7) (2014) 4129–4136, pMID: 24387600. arXiv:https://doi.org/https://doi.org/10.1021/es4037012.

[28] Y. Cui, X.-Y. Liu, T.-S. Chung, Enhanced osmotic energy generation from salinity gradients by modifying thin film composite membranes, Chem. Eng. J. 242 (2014) 195–203, https://doi.org/10.1016/j.cej.2013.12.078. URL, https://www.sciencedirect.com/science/article/pii/S1385894713016598.

[29] Y. Li, R. Wang, S. Qi, C. Tang, Structural stability and mass transfer properties of pressure retarded osmosis (PRO) membrane under high operating pressures, J. Membr. Sci. 488 (2015) 143–153, https://doi.org/10.1016/j.memsci.2015.04.030. URL, https://www.sciencedirect.com/science/article/pii/S0376738815003610.

[30] G. Han, S. Zhang, X. Li, T.-S. Chung, High performance thin film composite pressure retarded osmosis (PRO) membranes for renewable salinity-gradient energy generation, J. Membr. Sci. 440 (2013) 108–121, https://doi.org/10.1016/j.memsci.2013.04.001. URL, https://www.sciencedirect.com/science/article/pii/S0376738813002810.

[31] L.A. Hoover, J.D. Schiffman, M. Elimelech, Nanofibers in thin-film composite membrane support layers: enabling expanded application of forward and pressure retarded osmosis, Desalination 308 (2013) 73–81, new Directions in Desalination, https://doi.org/10.1016/j.desal.2012.07.019. URL, https://www.sciencedirect.com/science/article/pii/S0011916412003906.

[32] Y. Liang, Review of analytical and numerical modeling for pressure retarded osmosis membrane systems, Desalination 560 (2023) 116655, https://doi.org/10.1016/j.desal.2023.116655. URL, https://www.sciencedirect.com/science/article/pii/S0011916423002874.

[33] J.H. Low, J. Zhang, W.P. Li, T. Yang, C.F. Wan, F. Esa, M.S. Qua, K. Mottaiyan, S. Murugan, M. Aiman, A. Dhalla, T.-S. Chung, C. Gudipati, Industrial scale thin-

film composite membrane modules for salinity-gradient energy harvesting through pressure retarded osmosis, Desalination 548 (2023) 116217, https://doi.org/10.1016/j.desal.2022.116217. URL, https://www.sciencedirect.com/science/article/pii/S0011916422006725.
[34] B.A. Abdelkader, D.R. Navas, M.H. Sharqawy, A novel spiral wound module design for harvesting salinity gradient energy using pressure retarded osmosis, Renew. Energy 203 (2023) 542–553, https://doi.org/10.1016/j.renene.2022.12.073. URL, https://www.sciencedirect.com/science/article/pii/S0960148122018699.
[35] S.H. Chae, H. Rho, S. Moon, Modeling study of the effects of intrinsic membrane parameters on dilutive external concentration polarization occurring during forward and pressure-retarded osmosis, Desalination 569 (2024) 117043, https://doi.org/10.1016/j.desal.2023.117043. URL, https://www.sciencedirect.com/science/article/pii/S0011916423006756.
[36] R.R. Gonzales, A. Abdel-Wahab, S. Adham, D.S. Han, S. Phuntsho, W. Suwaileh, N. Hilal, H.K. Shon, Salinity gradient energy generation by pressure retarded osmosis: a review, Desalination 500 (2021) 114841, https://doi.org/10.1016/j.desal.2020.114841. URL, https://www.sciencedirect.com/science/article/pii/S0011916420315198.
[37] H. Manzoor, M.A. Selam, S. Adham, H.K. Shon, M. Castier, A. Abdel-Wahab, Energy recovery modeling of pressure-retarded osmosis systems with membrane modules compatible with high salinity draw streams, Desalination 493 (2020) 114624, https://doi.org/10.1016/j.desal.2020.114624. URL, https://www.sciencedirect.com/science/article/pii/S0011916420313023.
[38] Y. Wang, W. He, H. Zhu, Computational fluid dynamics (cfd) based modelling of osmotic energy generation using pressure retarded osmosis (pro), Desalination 389 (2016) 98–107, pressure Retarded Osmosis, https://doi.org/10.1016/j.desal.2016.02.002. URL, https://www.sciencedirect.com/science/article/pii/S0011916416300406.
[39] J. Benjamin, S.A.L. Mashrafi, A. Tejada-Martinez, N. Diaz-Elsayed, M.E. Arias, Q. Zhang, Optimizing pressure retarded osmosis spacer geometries: an experimental and CFD modeling study, J. Membr. Sci. 647 (2022) 120284, https://doi.org/10.1016/j.memsci.2022.120284. URL, https://www.sciencedirect.com/science/article/pii/S0376738822000333.
[40] M. Javadi Azad, A. Pouranfard, D. Emadzadeh, W. Lau, E. Alipanahpour Dil, Simulation of forward osmosis and pressure retarded osmosis membrane performance: effect of TiO2 nanoparticles loading on the semi-permeable membrane, Comput. Chem. Eng. 160 (2022) 107709, https://doi.org/10.1016/j.compchemeng.2022.107709. URL, https://www.sciencedirect.com/science/article/pii/S0098135422000527.
[41] F. Aschmoneit, C. Hélix-Nielsen, Submerged-helical module design for pressure retarded osmosis: a conceptual study using computational fluid dynamics, J. Membr. Sci. 620 (2021) 118704, https://doi.org/10.1016/j.memsci.2020.118704. URL, https://www.sciencedirect.com/science/article/pii/S0376738820312801.
[42] Z.M. Binger, A. Achilli, Surrogate modeling of pressure loss & mass transfer in membrane channels via coupling of computational fluid dynamics and machine learning, Desalination 548 (2023) 116241, https://doi.org/10.1016/j.desal.2022.116241. URL, https://www.sciencedirect.com/science/article/pii/S0011916422006968.
[43] A. Ruiz-García, I. Nuez, Simulation-based assessment of safe operating windows and optimization in full-scale seawater reverse osmosis systems, Desalination 533 (2022) 115768, https://doi.org/10.1016/j.desal.2022.115768. URL, https://www.sciencedirect.com/science/article/pii/S0011916422002235.
[44] S.M. Matta, M.A. Selam, H. Manzoor, S. Adham, H.K. Shon, M. Castier, A. Abdel-Wahab, Predicting the performance of spiral-wound membranes in pressure-retarded osmosis processes, Renew. Energy 189 (2022) 66–77, https://doi.org/10.1016/j.renene.2022.02.125. URL, https://www.sciencedirect.com/science/article/pii/S0960148122002749.
[45] K. Touati, F. Tadeo, H. Elfil, Osmotic energy recovery from reverse osmosis using two-stage pressure retarded osmosis, Energy 132 (2017) 213–224, https://doi.org/10.1016/j.energy.2017.05.050. URL, https://www.sciencedirect.com/science/article/pii/S0360544217308071.
[46] K. Touati, J. Salamanca, F. Tadeo, H. Elfil, Energy recovery from two-stage SWRO plant using PRO without external freshwater feed stream: theoretical analysis, Renew. Energy 105 (2017) 84–95, https://doi.org/10.1016/j.renene.2016.12.030. URL, https://www.sciencedirect.com/science/article/pii/S0960148116310783.
[47] J.M. Salamanca, O. Ãlvarez Silva, F. Tadeo, Potential and analysis of an osmotic power plant in the Magdalena River using experimental field-data, Energy 180 (2019) 548–555, https://doi.org/10.1016/j.energy.2019.05.048. URL, https://www.sciencedirect.com/science/article/pii/S0360544219309119.
[48] E.I. Obode, A. Badreldin, S. Adham, M. Castier, A. Abdel-Wahab, Techno-economic analysis towards full-scale pressure retarded osmosis plants, Energies 16 (1) (2023), https://doi.org/10.3390/en16010325.
[49] N. AlZainati, S. Yadav, A. Altaee, S. Subbiah, S.J. Zaidi, J. Zhou, R.A. Al-Juboori, Y. Chen, M.H. Shaheed, Impact of hydrodynamic conditions on optimum power generation in dual stage pressure retarded osmosis using spiral-wound membrane, Energy Nexus 5 (2022) 100030, https://doi.org/10.1016/j.nexus.2021.100030. URL, https://www.sciencedirect.com/science/article/pii/S2772427121000309.
[50] N. Al-Zainati, I. Ibrar, A. Altaee, S. Subbiah, J. Zhou, Multiple staging of pressure retarded osmosis: impact on the energy generation, Desalination 573 (2024) 117199, https://doi.org/10.1016/j.desal.2023.117199. URL, https://www.sciencedirect.com/science/article/pii/S0011916423008317.
[51] Y. Tanaka, M. Yasukawa, S. Goda, H. Sakurai, M. Shibuya, T. Takahashi, M. Kishimoto, M. Higa, H. Matsuyama, Experimental and simulation studies of two types of 5-inch scale hollow fiber membrane modules for pressure-retarded osmosis, Desalination 447 (2018) 133–146, https://doi.org/10.1016/j.desal.2018.09.015. URL, https://www.sciencedirect.com/science/article/pii/S0011916417327753.
[52] C. Lee, S.H. Chae, E. Yang, S. Kim, J.H. Kim, I.S. Kim, A comprehensive review of the feasibility of pressure retarded osmosis: recent technological advances and industrial efforts towards commercialization, Desalination 491 (2020) 114501, https://doi.org/10.1016/j.desal.2020.114501. URL, https://www.sciencedirect.com/science/article/pii/S0011916420302174.
[53] N. Al-Zainati, S. Subbiah, S. Yadav, A. Altaee, P. Bartocci, I. Ibrar, J. Zhou, A. K. Samal, F. Fantozzi, Experimental and theoretical work on reverse osmosis - dual stage pressure retarded osmosis hybrid system, Desalination 543 (2022) 116099, https://doi.org/10.1016/j.desal.2022.116099. URL, https://www.sciencedirect.com/science/article/pii/S0011916422005549.
[54] Q. Wang, Z. Zhou, J. Li, Q. Tang, Y. Hu, Investigation of the reduced specific energy consumption of the RO-PRO hybrid system based on temperature-enhanced pressure retarded osmosis, J. Membr. Sci. 581 (2019) 439–452, https://doi.org/10.1016/j.memsci.2019.03.079. URL, https://www.sciencedirect.com/science/article/pii/S0376738819300407.
[55] B. Blankert, Y. Kim, H. Vrouwenvelder, N. Ghaffour, Facultative hybrid RO-PRO concept to improve economic performance of PRO: feasibility and maximizing efficiency, Desalination 478 (2020) 114268, https://doi.org/10.1016/j.desal.2019.114268. URL, https://www.sciencedirect.com/science/article/pii/S0011916419318831.
[56] S. Liu, W. Song, M. Meng, M. Xie, Q. She, P. Zhao, X. Wang, Engineering pressure retarded osmosis membrane bioreactor (PRO-MBR) for simultaneous water and energy recovery from municipal wastewater, Sci. Total Environ. 826 (2022) 154048, https://doi.org/10.1016/j.scitotenv.2022.154048. URL, https://www.sciencedirect.com/science/article/pii/S0048969722011408.
[57] S. Lin, N.Y. Yip, T.Y. Cath, C.O. Osuji, M. Elimelech, Hybrid pressure retarded osmosis–membrane distillation system for power generation from low-grade heat: thermodynamic analysis and energy efficiency, Environ. Sci. Technol. 48 (9) (2014) 5306–5313, pMID: 24724732. arXiv:https://doi.org/https://doi.org/10.1021/es405173b.
[58] A.E. Zadeh, K. Touati, C.N. Mulligan, J.R. McCutcheon, M.S. Rahaman, Closed-loop pressure retarded osmosis draw solutions and their regeneration processes: a review, Renew. Sust. Energ. Rev. 159 (2022) 112191, https://doi.org/10.1016/j.rser.2022.112191. URL, https://www.sciencedirect.com/science/article/pii/S1364032122001150.
[59] T.T. Tran, K. Park, A.D. Smith, System scaling approach and thermoeconomic analysis of a pressure retarded osmosis system for power production with hypersaline draw solution: a great salt lake case study, Energy 126 (2017) 97–111, https://doi.org/10.1016/j.energy.2017.03.002. URL, https://www.sciencedirect.com/science/article/pii/S0360544217303602.
[60] N. Bajraktari, C. Hélix-Nielsen, H.T. Madsen, Pressure retarded osmosis from hypersaline sources - a review, Desalination 413 (2017) 65–85, https://doi.org/10.1016/j.desal.2017.02.017. URL, https://www.sciencedirect.com/science/article/pii/S0011916416320549.
[61] J. Lee, Y. Shin, J. Kim, S. Hong, Feasibility and challenges of high-pressure pressure retarded osmosis applications utilizing seawater and hypersaline water sources, Desalination 581 (2024) 117578, https://doi.org/10.1016/j.desal.2024.117578. URL, https://www.sciencedirect.com/science/article/pii/S0011916424002893.
[62] N.Y. Yip, A. Tiraferri, W.A. Phillip, J.D. Schiffman, L.A. Hoover, Y.C. Kim, M. Elimelech, Thin-film composite pressure retarded osmosis membranes for sustainable power generation from salinity gradients, Environ. Sci. Technol. 45 (10) (2011) 4360–4369, pMID: 21491936. arXiv:https://doi.org/https://doi.org/10.1021/es104325z.
[63] S. Loeb, Production of energy from concentrated brines by pressure-retarded osmosis: I. Preliminary technical and economic correlations, J. Membr. Sci. 1 (1976) 49–63, https://doi.org/10.1016/S0376-7388(00)82257-7. URL, https://www.sciencedirect.com/science/article/pii/S0376738800822577.
[64] S. Phuntsho, S. Hong, M. Elimelech, H.K. Shon, Osmotic equilibrium in the forward osmosis process: modelling, experiments and implications for process performance, J. Membr. Sci. 453 (2014) 240–252, https://doi.org/10.1016/j.memsci.2013.11.009. URL, https://www.sciencedirect.com/science/article/pii/S0376738813008946.
[65] K. Lee, R. Baker, H. Lonsdale, Membranes for power generation by pressure-retarded osmosis, J. Membr. Sci. 8 (2) (1981) 141–171, https://doi.org/10.1016/S0376-7388(00)82088-8. URL, https://www.sciencedirect.com/science/article/pii/S0376738800820888.
[66] C.H. Tan, H.Y. Ng, Revised external and internal concentration polarization models to improve flux prediction in forward osmosis process, Desalination 309 (2013) 125–140, https://doi.org/10.1016/j.desal.2012.09.022. URL, https://www.sciencedirect.com/science/article/pii/S0011916412005267.
[67] V. Geraldes, N.E. Pereira, M.N. de Pinho, Simulation and optimization of medium-sized seawater reverse osmosis processes with spiral-wound modules, Ind. Eng. Chem. Res. 44 (6) (2005) 1897–1905, https://doi.org/10.1021/ie049357s. URL doi:10.1021/ie049357s.
[68] D. Attarde, M. Jain, K. Chaudhary, S.K. Gupta, Osmotically driven membrane processes by using a spiral wound module — modeling, experimentation and numerical parameter estimation, Desalination 361 (2015) 81–94, https://doi.org/10.1016/j.desal.2015.01.025. URL, https://www.sciencedirect.com/science/article/pii/S0011916415000442.

[69] G. Schock, A. Miquel, Mass transfer and pressure loss in spiral wound modules, Desalination 64 (1987) 339–352, https://doi.org/10.1016/0011-9164(87)90107-X. URL, https://www.sciencedirect.com/science/article/pii/001191648790107X.
[70] M.H. Sharqawy, J.H. Lienhard V, S.M. Zubair, On exergy calculations of seawater with applications in desalination systems, Int. J. Therm. Sci. 50 (2) (2011) 187–196, https://doi.org/10.1016/j.ijthermalsci.2010.09.013. URL, https://www.sciencedirect.com/science/article/pii/S1290072910002784.
[71] A. Altaee, N. Hilal, Design optimization of high performance dual stage pressure retarded osmosis, Desalination 355 (2015) 217–224, https://doi.org/10.1016/j.desal.2014.11.002. URL, https://www.sciencedirect.com/science/article/pii/S0011916414005815.